

Acoustic axes in weak triclinic anisotropy

Václav Vavryčuk

Geophysical Institute, Academy of Sciences of the Czech Republic, Boční II, 141 31 Praha 4, Czech Republic. E-mail: vv@ig.cas.cz

Accepted 2005 July 26. Received 2005 June 29; in original form 2005 January 12

SUMMARY

Acoustic axes can exist even under an infinitesimally weak anisotropy, and occur when slowness surfaces of the $S1$ and $S2$ waves touch or intersect. The maximum number of isolated acoustic axes in weak triclinic anisotropy is 16 as in strong triclinic anisotropy. The directions of acoustic axes are calculated by solving two coupled polynomial equations in two variables. The order of the equations is 6 under strong anisotropy and reduces to 5 under weak anisotropy. The weak anisotropy approximation is particularly useful, when calculating the acoustic axes under extremely weak anisotropy with anisotropy strength less than 0.1 per cent because the equations valid for strong anisotropy might become numerically unstable and their modification, which stabilizes them, is complicated. The weak anisotropy approximation can also find applications in inversions for anisotropy from the directions of acoustic axes.

Key words: elastic-wave theory, perturbation methods, polarization, seismic anisotropy, seismic-wave propagation, shear-wave splitting.

1 INTRODUCTION

Acoustic axes (singularities, degeneracies) are directions in anisotropic media, in which phase velocities of two or three plane waves (P , $S1$ or $S2$ waves) coincide. We distinguish several types of acoustic axes (Khatkevich 1963; Fedorov 1968; Khatkevich 1977; Alshits & Lothe 1979a; Crampin & Yedlin 1981; Grechka & Obolentseva 1993; Helbig 1994): they can form either single isolated points classified as kiss, conical or wedge singularities, or they can combine into line singularities. The most frequent acoustic axis in triclinic anisotropy is conical, which is classified as the stable singularity. On the other hand, the kiss, wedge and line singularities are called unstable, because they disappear or split into several conical singularities if the medium is a subject of a small perturbation of elastic parameters.

Acoustic axes are very important, because they cause singularities in the field of polarization vectors (Alshits & Lothe 1979b; Alshits *et al.* 1985). The singular behaviour of the polarization field near an acoustic axis depends on its type (see Fig. 1) and is quantified by the topological charge of the singularity (Shuvalov 1998). The acoustic axes can also cause anomalies in the shape of the slowness and wave surfaces. This is manifested by the existence of parabolic lines on the slowness surface (Vavryčuk 2003a), which are mapped onto caustics and anti-caustics on the wave surface (see Fig. 2). The caustics cause triplications and strong energy focusing (Hurley & Wolfe 1985; Every 1986, 1988; Shuvalov & Every 1997; Wolfe 1998). The acoustic axes also pose complications in tracing rays (Vavryčuk 2001, 2003b; Farra 2005) and in modelling wavefields because of the coupling of waves (Chapman & Shearer 1989; Kravtsov & Orlov 1990; Coates & Chapman 1990; Rümpker & Thomson 1994; Pšenčík 1998; Bulant & Klimeš 2004; Klimeš & Bulant 2004).

The maximum number of isolated acoustic axes is 16 in triclinic anisotropy (Holm 1992; Darinskii 1994; Alshits & Lothe 2004; Vavryčuk 2005) similarly as in monoclinic, orthorhombic and trigonal symmetry (Khatkevich 1963; Musgrave 1985; Boulanger & Hayes 1998; Mozhaev *et al.* 2001). However, the calculation of the directions of the acoustic axes in triclinic anisotropy is more involved than in anisotropy of higher symmetry. While acoustic axes in monoclinic symmetry are calculated by solving one polynomial equation of the sixth order in one variable, the acoustic axes in triclinic anisotropy are calculated by solving two coupled polynomial equations of the sixth order in two variables. Obviously this implies that the positions of acoustic axes are complicated functions of anisotropy parameters (Vavryčuk 2005).

In general, anomalies observed in the directions of acoustic axes and in their vicinities appear, or they are more pronounced, under strong rather than weak anisotropy. For example, we can observe acoustic axes of the P and $S1$ waves or triple acoustic axes of the P , $S1$ and $S2$ waves under strong anisotropy, but only the acoustic axes of the $S1$ and $S2$ waves can be observed under weak anisotropy. Also triplications of the wave surface appear more frequently under strong rather than weak anisotropy. Under weak anisotropy, the shapes of slowness and wave surfaces and the behaviour of waves are usually much simpler and modelling of propagating waves is much easier (Jech & Pšenčík 1989; Farra 2001, 2004, 2005; Vavryčuk 2003a, 2005). Importantly, weak anisotropy is not only a useful theoretical concept simplifying modelling of waves, but it is also a reasonable assumption valid for many real materials including most rocks and geological structures in the Earth (Thomsen 1986; Babuška & Cara 1991; Savage 1999). Therefore, I shall focus in this paper on studying the number and properties of acoustic axes in weak triclinic anisotropy. I shall apply the perturbation theory (Jech & Pšenčík 1989; Farra 2001; Vavryčuk

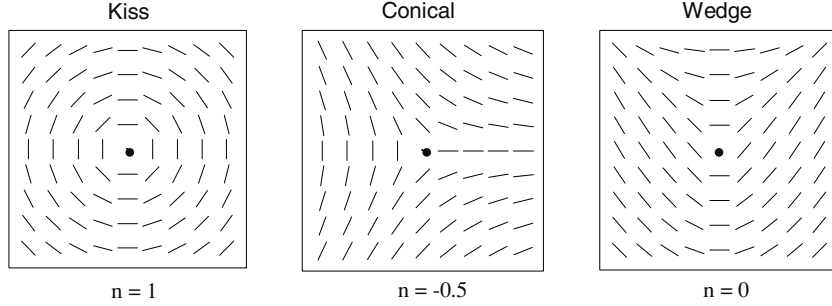
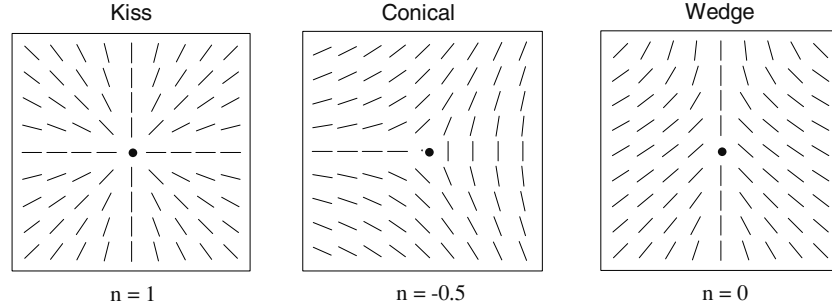
S1 wave**S2 wave**

Figure 1. The field of polarization vectors on the slowness surfaces near a kiss, conical and wedge acoustic axis for the $S1$ and $S2$ waves. The polarization vectors are projected into the plane perpendicular to the acoustic axis. The field of polarization vectors is singular in the acoustic axis. The topological charge n of the singularities is $+1, -1/2$ and 0 . The dot marks the position of the singularity.

2003a) to check whether a rather complicated calculation of the number and directions of acoustic axes in triclinic anisotropy simplifies under weak anisotropy. I shall try to find specific properties of acoustic axes in weak anisotropy and to resolve whether the maximum number of acoustic axes is reduced under weak anisotropy or not.

2 ACOUSTIC AXES IN STRONG ANISOTROPY

2.1 System of equations

The Christoffel tensor $\Gamma(\mathbf{n})$ is defined as (Fedorov 1968; Musgrave 1970; Červený 2001)

$$\Gamma_{jk}(\mathbf{n}) = a_{ijkl}n_i n_l, \quad (1)$$

where $a_{ijkl} = c_{ijkl}/\rho$ are the density-normalized elastic parameters, c_{ijkl} are the elastic parameters, ρ is the density of the medium, and \mathbf{n} is the unit vector defining the slowness direction. The Einstein summation convention over repeated subscripts is applied. For physically realizable media, the elastic parameters a_{ijkl} satisfy the stability conditions (Helbig 1994, eqs 5.5–5.10) and the Christoffel tensor $\Gamma(\mathbf{n})$ is positive-definite for all directions \mathbf{n} . The Christoffel tensor $\Gamma(\mathbf{n})$ has three eigenvalues $G^{(M)}$ and three unit eigenvectors $\mathbf{g}^{(M)}$, which are calculated from

$$\Gamma_{jk}g_k^{(M)} = G^{(M)}g_j^{(M)}, \quad M = 1, 2, 3, \quad (2)$$

where M denotes the type of wave (P , $S1$ or $S2$). The eigenvalue corresponds to the squared phase velocity, $G = c^2$, and the eigenvector describes the polarization vector of the wave. Using the spectral decomposition of $\Gamma(\mathbf{n})$ and applying the condition for the acoustic

axis, $G^{(2)} = G^{(3)}$, we obtain

$$\Gamma_{jk} = (G^{(1)} - G^{(2)}) g_j^{(1)} g_k^{(1)} + G^{(2)} \delta_{jk}, \quad (3)$$

where δ_{jk} is the Kronecker delta. If $G^{(1)} > G^{(2)} = G^{(3)}$, the $S1$ and $S2$ phase velocities coincide at the acoustic axis, if $G^{(1)} < G^{(2)} = G^{(3)}$, the P and $S1$ phase velocities coincide at the acoustic axis. Eq. (3) can be expressed as follows (Darinskii 1994):

$$a_{ijkl}s_i s_l = g_j g_k + \delta_{jk}, \quad (4)$$

where $\mathbf{s} = \mathbf{n}/\sqrt{G^{(2)}}$ is the slowness vector of the degenerate wave and $\mathbf{g} = \mathbf{g}^{(1)}\sqrt{(G^{(1)} - G^{(2)})/G^{(2)}}$ is an eigenvector of the non-degenerate wave of a generally non-unit length. Vectors \mathbf{s} and \mathbf{g} may be real or complex valued. Eq. (4) is a system of six quadratic equations in six unknowns: $\mathbf{s} = (s_1, s_2, s_3)^T$ and $\mathbf{g} = (g_1, g_2, g_3)^T$. The number of solutions is $2^6 = 64$. If we take into account that solutions of different signs: $\pm\mathbf{s}$, $\pm\mathbf{g}$, correspond to the same acoustic axis, the maximum number of acoustic axes is reduced from 64 to 16. This number comprises the solutions with real-valued as well as complex-valued slowness vector \mathbf{s} . The real-valued solutions correspond to acoustic axes of homogeneous plane waves propagating in anisotropic media, the complex-valued solutions correspond to acoustic axes of inhomogeneous plane waves. Both types of acoustic axes differ mainly in their polarization field. While the polarization is linear near the real acoustic axis, it becomes elliptical near the complex acoustic axis (see Shuvalov 2001; Vavryčuk 2005).

Eliminating eigenvalues and eigenvectors in eq. (3), we obtain (Darinskii 1994):

$$\Gamma_{11} - \frac{\Gamma_{12}\Gamma_{13}}{\Gamma_{23}} = \Gamma_{22} - \frac{\Gamma_{12}\Gamma_{23}}{\Gamma_{13}} = \Gamma_{33} - \frac{\Gamma_{13}\Gamma_{23}}{\Gamma_{12}}, \quad (5)$$

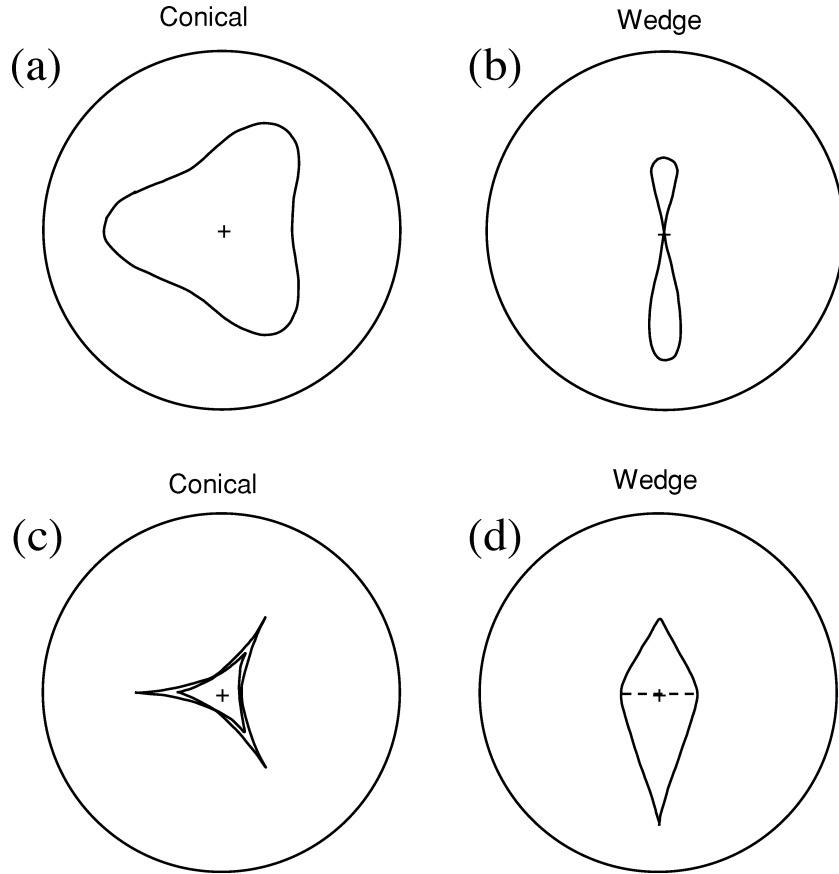


Figure 2. Parabolic lines (upper plots) and caustics (lower plots) for the S2 wave near the conical and wedge singularities. The conical singularity lies along the direction $\mathbf{n} = \frac{1}{\sqrt{3}}(1, 1, 1)^T$ in cubic anisotropy with parameters (in $\text{km}^2 \text{ s}^{-2}$): $a_{11} = a_{22} = a_{33} = 6$, $a_{44} = a_{55} = a_{66} = 2$, $a_{12} = a_{13} = a_{23} = 2.3$. The wedge singularity lies along the vertical axis in monoclinic anisotropy arisen from the above cubic anisotropy by considering additional non-zero elastic parameter $a_{14} = 0.03 \text{ km}^2 \text{ s}^{-2}$. The plus signs in (a) and (b) mark the acoustic axes. Equal area projection is used. The bounding circles correspond to the deviation of: (a) 4.0° , (b) 3.0° , (c) 2.1° and (d) 2.0° from the singularity. The dashed straight line in (d) marks the anti-caustic generated by the wedge singularity. The anti-caustic generated by the conical singularity coincides with the bounding circle in (c).

and consequently (Khatkevich 1963):

$$(\Gamma_{11} - \Gamma_{22})\Gamma_{13}\Gamma_{23} - \Gamma_{12}(\Gamma_{13}^2 - \Gamma_{23}^2) = 0, \quad (6a)$$

$$(\Gamma_{11} - \Gamma_{33})\Gamma_{12}\Gamma_{23} - \Gamma_{13}(\Gamma_{12}^2 - \Gamma_{23}^2) = 0, \quad (6b)$$

$$(\Gamma_{22} - \Gamma_{33})\Gamma_{12}\Gamma_{13} - \Gamma_{23}(\Gamma_{12}^2 - \Gamma_{13}^2) = 0. \quad (6c)$$

Eqs (6a–c) are suitable for calculating the acoustic axes numerically. They represent a system of sixth-order equations in three unknown components of the unit direction vector \mathbf{n} : n_1 , n_2 and n_3 . The three eqs (6a–c) are not independent, hence we solve only two of them. We obtain 72 solutions, which are generally complex valued. Taking into account that $\pm\mathbf{n}$ describes the same direction, the number of directions reduces from 72 to 36.

2.2 Spurious directions

Since eq. (4) yields only 16 acoustic axes, 20 of the 36 directions calculated from (6) must be spurious and do not describe acoustic axes. In fact, the spurious directions were incorporated into the

solution, when eq. (5) was multiplied by terms $\Gamma_{12}\Gamma_{13}$, $\Gamma_{12}\Gamma_{23}$ or $\Gamma_{13}\Gamma_{23}$ in order to derive eq. (6). Therefore, we should eliminate from the solutions of eqs (6a–c) the directions, for which one of the following three systems of equations is satisfied

$$\Gamma_{13} = 0 \text{ and } \Gamma_{23} = 0, \quad (7a)$$

$$\Gamma_{12} = 0 \text{ and } \Gamma_{23} = 0, \quad (7b)$$

$$\Gamma_{12} = 0 \text{ and } \Gamma_{13} = 0. \quad (7c)$$

Eqs (7a–c) describe three systems of quadratic equations, each of them having eight solutions which reduce to four directions, if different signs of \mathbf{n} are omitted. Hence, we obtained a total of 12 spurious directions. Furthermore, 8 of the 12 spurious directions appear in eq. (6) twice. Which eight spurious directions are doubled, depends on the pair of eqs (6a–c) we actually solve. For example, in solving eqs (6a–b), the solutions of eqs (7a–b) are doubled; in solving eqs (6b–c), the solutions of eqs (7b–c) are doubled. Hence, the total number of spurious directions in eq. (6) is 20. This confirms that only 16 acoustic axes can exist in triclinic anisotropy.

3 ACOUSTIC AXES IN WEAK ANISOTROPY

3.1 Weak anisotropy expansion

Weak triclinic anisotropy with elastic parameters a_{ijkl} is obtained by perturbing an isotropic medium in the following way:

$$a_{ijkl} = a_{ijkl}^0 + \varepsilon b_{ijkl}, \quad (8)$$

where

$$a_{ijkl}^0 = \lambda \delta_{ij} \delta_{kl} + \mu (\delta_{ik} \delta_{jl} + \delta_{il} \delta_{jk}). \quad (9)$$

Parameters λ and μ define the Lamé coefficients of an isotropic background medium, tensor b_{ijkl} defines the perturbations from isotropy into triclinic anisotropy, and ε is a small quantity which measures anisotropy strength. In order to keep ε within a reasonable range of values, it is advantageous to scale tensor b_{ijkl} to have a norm comparable to the norm of a_{ijkl}^0 . For any weak triclinic anisotropy described by tensor a_{ijkl} , the two parameters of the isotropic background medium can be chosen so that the perturbation tensor satisfies: $b_{3333} = 0$ and $b_{1212} = 0$. These constraints are applied in all the following equations to simplify them. In addition, it would be possible to impose zeros also to other three parameters of b_{ijkl} , supposing we confine ourselves to a specially oriented coordinate system. This constraint, however, is not applied here, because it would require finding this coordinate system for each studied triclinic anisotropy and evaluate the parameters in this system. Hence, here the weakly anisotropic triclinic medium is described by 21 elastic parameters, two of them define the isotropic background and 19 of them define the perturbation to anisotropy.

For $\varepsilon = 0$ in (8), weak anisotropy reduces to isotropy. The Christoffel tensor Γ in (1) is degenerate with eigenvalues $G^P = \lambda + 2\mu$ and $G^S \equiv G^{S1} = G^{S2} = \mu$, which are independent of direction \mathbf{n} . Consequently, the P - and S -wave slowness surfaces are fully detached, $G^P > G^S$, and the $S1$ and $S2$ waves have coincident phase velocities in all directions \mathbf{n} , $G^{S1} = G^{S2}$. For small non-zero ε , the P wave remains detached from the $S1$ and $S2$ waves, but the global degeneracy of the $S1$ and $S2$ waves is removed, and the phase velocities of the $S1$ and $S2$ waves can coincide only in selected directions (see Fig. 3). Hence, under weak anisotropy we can observe acoustic axes of the $S1$ and $S2$ waves, but not the acoustic axes of the P and $S1$ waves, or the triple acoustic axes of the P , $S1$ and $S2$ waves.

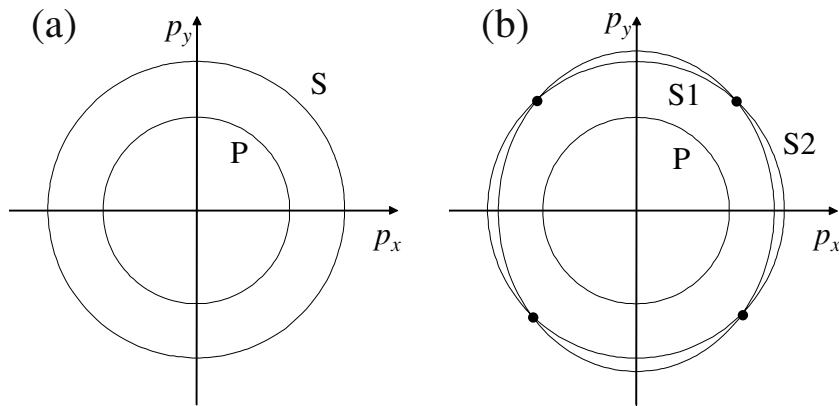


Figure 3. A sketch of slowness surfaces for P and S waves for isotropic media (a) and for P , $S1$ and $S2$ waves for weakly anisotropic media (b). The dots in (b) mark the positions of the acoustic axes.

3.2 System of equations

Inserting the Christoffel tensor Γ specified under weak anisotropy (see Appendix A) into eqs (6a–c) we obtain:

$$\begin{aligned} & \varepsilon(\lambda + \mu)^2 P_1(b_{ijkl}, n_1, n_2, n_3) \\ & + \varepsilon^2(\lambda + \mu) P_2(b_{ijkl}, n_1, n_2, n_3) \\ & + \varepsilon^3 P_3(b_{ijkl}, n_1, n_2, n_3) = 0, \end{aligned} \quad (10a)$$

$$\begin{aligned} & \varepsilon(\lambda + \mu)^2 Q_1(b_{ijkl}, n_1, n_2, n_3) \\ & + \varepsilon^2(\lambda + \mu) Q_2(b_{ijkl}, n_1, n_2, n_3) \\ & + \varepsilon^3 Q_3(b_{ijkl}, n_1, n_2, n_3) = 0, \end{aligned} \quad (10b)$$

$$\begin{aligned} & \varepsilon(\lambda + \mu)^2 R_1(b_{ijkl}, n_1, n_2, n_3) \\ & + \varepsilon^2(\lambda + \mu) R_2(b_{ijkl}, n_1, n_2, n_3) \\ & + \varepsilon^3 R_3(b_{ijkl}, n_1, n_2, n_3) = 0, \end{aligned} \quad (10c)$$

where polynomials P_1 , Q_1 and R_1 are of the first order, polynomials P_2 , Q_2 and R_2 are of the second order, and P_3 , Q_3 and R_3 are polynomials of the third order in b_{ijkl} . Eqs (10a–c) contain only perturbation terms, because eqs (6a–c) are automatically satisfied for any isotropic background.

If we assume $\varepsilon/(\lambda + \mu) \rightarrow 0$ (but not equal to zero), we can neglect the higher-order terms in ε in eqs (10a–c) and retain only the linear terms in ε . Note that, it is not sufficient to impose only condition $\varepsilon \rightarrow 0$, because for $\lambda + \mu \approx \varepsilon$ all three terms in eqs (10a–c) are significant and none of them can be neglected. Applying condition $\varepsilon/(\lambda + \mu) \rightarrow 0$, we obtain:

$$P_1(b_{ijkl}, n_1, n_2, n_3) = 0, \quad (11a)$$

$$Q_1(b_{ijkl}, n_1, n_2, n_3) = 0, \quad (11b)$$

$$R_1(b_{ijkl}, n_1, n_2, n_3) = 0. \quad (11c)$$

Polynomials P_1 , Q_1 and R_1 are homogeneous polynomials of the sixth order n_1 , n_2 and n_3 . They can be expressed as follows:

$$\begin{aligned} P_1 &= n_3 p_{ij} n_1^i n_2^j n_3^{5-i-j}, \\ Q_1 &= n_2 q_{ij} n_1^i n_2^j n_3^{5-i-j}, \\ R_1 &= n_1 r_{ij} n_1^i n_2^j n_3^{5-i-j}, \end{aligned} \quad (12)$$

where summation over repeated indices is applied. Indices i and j run from 0 to 5, and their sum is less than or equal to 5. Coefficients p_{ij} , q_{ij} and r_{ij} are presented in Appendix B. If we choose a coordinate system, in which no acoustic axis lies in the coordinate planes, then eqs (11a–c) simplify as follows

$$p_{ij}n_1^i n_2^j n_3^{5-i-j} = 0, \quad (13a)$$

$$q_{ij}n_1^i n_2^j n_3^{5-i-j} = 0, \quad (13b)$$

$$r_{ij}n_1^i n_2^j n_3^{5-i-j} = 0. \quad (13c)$$

The equations are homogeneous polynomial equations of the fifth order in three unknown components of the unit vector \mathbf{n} . The equations can be transformed into inhomogeneous polynomial equations of the fifth order in two unknowns u and v :

$$p_{ij}u^i v^j = 0, \quad (14a)$$

$$q_{ij}u^i v^j = 0, \quad (14b)$$

$$r_{ij}u^i v^j = 0, \quad (14c)$$

where $u = n_1/n_3$ and $v = n_2/n_3$. Using this substitution, we reject all solutions in the x_1-x_2 plane ($n_3 = 0$). Indices i and j run from 0 to 5 and their sum is less than or equal to 5. If some acoustic axes lie in the x_1-x_2 plane or in the other coordinate planes, the medium must be rotated to avoid this specific situation.

Eqs (14a–c) are not independent, hence we solve only two of them. In solving any two equations of (14a–c), we obtain 22 real- or complex-valued solutions, which comprise the true acoustic axes as well as the spurious directions.

3.3 Spurious directions

To identify and eliminate the spurious directions from the solutions of eqs (14a–c), we have to solve complementary equations similar to eqs (7a–c) designed for strong anisotropy. Expressing the Christoffel tensor in (7a–c) for weak anisotropy and keeping the leading terms only, we obtain the following three systems of equations:

$$(\lambda + \mu)n_1n_3 = 0 \quad \text{and} \quad (\lambda + \mu)n_2n_3 = 0, \quad (15a)$$

$$(\lambda + \mu)n_1n_2 = 0 \quad \text{and} \quad (\lambda + \mu)n_2n_3 = 0, \quad (15b)$$

$$(\lambda + \mu)n_1n_2 = 0 \quad \text{and} \quad (\lambda + \mu)n_1n_3 = 0. \quad (15c)$$

The equations imply that the spurious solutions must lie in the coordinate planes. Since eqs (14a–c) yield solutions out of the x_1-x_2 plane, the spurious directions can lie only in the two other coordinate planes: x_1-x_3 and x_2-x_3 . It can be proved that each coordinate plane contains three spurious solutions, so that a total of six spurious solutions is obtained in solving eqs (14a–c).

Hence, if we calculate the acoustic axes by solving eqs (14a–c), we obtain 22 solutions from which we have to eliminate six spurious directions, which lie in the coordinate planes x_1-x_3 and x_2-x_3 . We thus find that the maximum number of acoustic axes in weak triclinic anisotropy is 16. This implies that weak triclinic anisotropy is characterized by the same maximum number of acoustic axes as strong triclinic anisotropy.

The existence of weak triclinic anisotropy with 16 acoustic axes can be illustrated on the example of anisotropy defined by the following perturbation matrix:

$$\mathbf{B} = \begin{bmatrix} -0.35 & -0.52 & -0.02 & -0.01 & 0.22 & -0.01 \\ & -0.57 & -0.04 & -0.02 & 0.43 & -0.01 \\ & & 0 & 0.01 & 0.26 & -0.01 \\ & & & -0.59 & -0.01 & 0.21 \\ & & & & -0.55 & 0.01 \\ & & & & & 0 \end{bmatrix}, \quad (16)$$

which expresses tensor b_{ijkl} in the two-index notation (see Musgrave 1970, eq. 3.13.4). This anisotropy has 16 acoustic axes not only for infinitesimally small anisotropy strength (see Fig. 4), but also for anisotropy with ε up to 0.2 assuming $\lambda = 1$ and $\mu = 1$ in eqs (8–9). For higher values of ε , the number of real acoustic axes is reduced. Also the positions of the acoustic axes on the sphere can change with ε (see Vavryčuk 2005). The isotropic background $\lambda = 1$ and $\mu = 1$ (with no specified units) was used just for simplicity. Obviously, the anisotropy example can easily be rescaled to values more appropriate in geophysics.

3.4 Numerical calculation of acoustic axes

The exact directions of acoustic axes in weak as well as strong triclinic anisotropy can be conveniently calculated by solving modified eqs (10a–c). The modification lies in dividing (10a–c) by ε . These are homogeneous polynomial equations of the sixth order in three unknown components n_1 , n_2 and n_3 of the unit direction vector \mathbf{n} . Using the substitutions $u = n_1/n_3$ and $v = n_2/n_3$, we obtain inhomogeneous polynomial equations of the sixth order in unknowns u and v . The roots of the equations can be calculated, for example, using Gröbner bases (Fröberg 1997), implemented in symbolic algebra packages. Solving modified eqs (10a–c) we obtain 36 solutions, from which we have to exclude 20 spurious solutions defined by eqs (7a–c). To identify and eliminate the spurious solutions, we

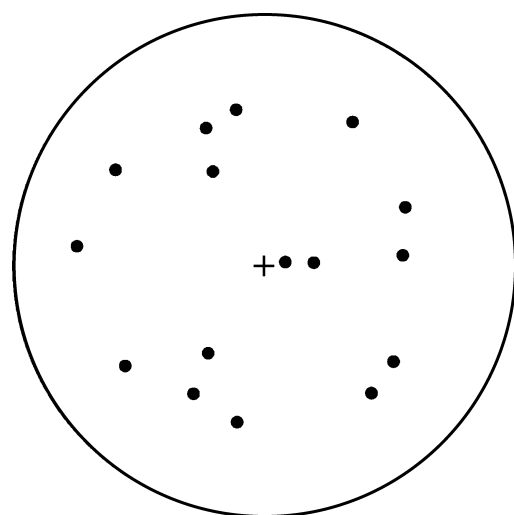


Figure 4. A polar plot of positions of acoustic axes for a weak triclinic anisotropy with 16 acoustic axes. The vertical axis is marked by the plus sign. The points at the bounding circle correspond to horizontal directions. For anisotropy parameters b_{ijkl} , see (16). Other parameters: $\lambda = 1$, $\mu = 1$, and $\varepsilon = 0.01$. Equal-area projection is used.

can either solve eqs (7a–c) or we can simply check, at which of the 36 directions calculated from eqs (10a–c) the Christoffel tensor is non-degenerate. Using this approach, we obtain the exact real as well as complex acoustic axes in triclinic media with any strength of anisotropy. On the contrary, eqs (6a–c), which are equivalent to eqs (10a–c), are suitable for calculating acoustic axes under strong rather than weak anisotropy. The reason is that eqs (6a–c) can fail if triclinic anisotropy is extremely weak. In this case, the left-hand sides of eqs (6a–c) are very close to zero for all directions \mathbf{n} , and the solution can be distorted by numerical errors.

The *approximate directions* of acoustic axes in weak triclinic anisotropy can be conveniently calculated using eqs (14a–c). The spurious directions are eliminated by rejecting all solution lying in the coordinate planes. As mentioned, eqs (14a–c) are inhomogeneous polynomial equations of the fifth order in unknowns u and v . The roots of the equations can be calculated similarly as for strong anisotropy using Gröbner bases (Fröberg 1997), implemented in symbolic algebra packages. The weak anisotropy approximation has the following advantages: First, the fifth-order equations are solved faster than the sixth-order equations. Second, eqs (14a–c) are applicable to extremely weak anisotropy, where eqs (6a–c) become unstable. Third, eqs (14a–c) are much simpler and more easily to code than eqs (10a–c), which are also applicable to extremely weak anisotropy. The simplification originates in neglecting rather long and complex polynomials P_2 , Q_2 , R_2 , P_3 , Q_3 and R_3 . Fourth, eqs (14a–c) can be used for inversion for anisotropy from known directions of acoustic axes.

For media of higher symmetry, it is not convenient to use eqs (6a–c), (10a–c) or (14a–c) for finding the acoustic axes, because they are unnecessarily complicated and they may even fail when the true or spurious solutions are not isolated. Instead, much simpler systems of algebraic equations designed for each specific symmetry are used (Boulanger & Hayes 1998).

Finally, it should also be mentioned that the acoustic axes can be calculated using a direct numerical approach. This approach is based on minimizing the square of the difference between numerically calculated eigenvalues of the Christoffel tensor. The minimization can be performed using some standard inversion techniques like the gradient method. Since the misfit function has several minima, we have to invert repeatedly for varying initial guesses of the position of the acoustic axis. Not to skip some solutions, the initial positions of the acoustic axes should cover the whole hemisphere in a regular grid and the grid should be sufficiently dense. This approach is applicable to any type of anisotropy with isolated acoustic axes. It is also reasonably fast and accurate provided that anisotropy is not extremely weak. However, it does not yield complex acoustic axes and sometimes it may skip some solutions, for example, in situations, when two acoustic axes are very close each to the other.

4 APPLICATION TO ROCKS

In this section, the proposed algorithm for calculating the acoustic axes in weak triclinic anisotropy is applied to observations of anisotropy on rocks. I consider anisotropy of four rock samples (see Weiss *et al.* 1999, Table 1): metapelite I, metapelite II, granulite and si-ga gneiss, which represent rocks in the lower continental Earth's crust. The samples originate from Calabria, Italy and the anisotropy was determined from texture data (see Siegesmund *et al.* 1996) using the Voigt average method. The elasticity tensors contain all 21 elastic parameters (see Table 1) and thus describe gen-

Table 1. Elastic parameters of rock samples.

Elastic parameters	Metapelite I	Metapelite II	Granulite	Si-ga gneiss
C_{11}	166.95	141.09	142.05	253.01
C_{22}	188.77	150.57	131.25	256.61
C_{33}	177.96	149.48	135.65	252.81
C_{44}	58.55	46.03	40.88	77.70
C_{55}	51.45	41.24	41.08	75.50
C_{66}	52.65	41.74	40.28	76.80
C_{12}	61.26	55.42	53.88	90.40
C_{13}	62.76	57.32	56.28	91.80
C_{14}	-0.50	-0.40	-1.20	0.30
C_{15}	-1.60	0.70	-0.90	0.00
C_{16}	0.60	1.40	-0.50	0.09
C_{23}	66.36	57.21	50.98	95.80
C_{24}	0.30	0.00	-0.80	-0.30
C_{25}	-0.10	0.50	-0.50	-0.10
C_{26}	0.30	1.90	0.60	-0.30
C_{34}	0.20	0.20	-0.10	-0.10
C_{35}	-0.30	1.80	-1.10	-0.10
C_{36}	0.30	0.60	-0.10	-0.20
C_{45}	-0.30	0.70	0.20	-0.10
C_{46}	-0.30	0.50	0.00	-0.10
C_{56}	0.20	-0.10	-0.10	-0.10

Elastic parameters C_{ij} are in $10^9 \text{ kg m}^{-1}\text{s}^{-2}$. The values of the elastic parameters were published by Weiss *et al.* (1999, Table 1).

Table 2. Velocity, anisotropy and acoustic axes of rock samples.

	Metapelite I	Metapelite II	Granulite	Si-ga gneiss
$v^P [\text{km s}^{-1}]$	7.6	7.1	6.9	8.4
$v^S [\text{km s}^{-1}]$	4.2	3.9	3.8	4.7
$\rho [10^3 \text{ kg m}^{-3}]$	3.06	2.88	2.87	3.55
$A^P [\text{per cent}]$	6.8	4.8	4.3	1.8
$A^{S1} [\text{per cent}]$	5.3	5.6	1.2	3.4
$A^{S2} [\text{per cent}]$	4.9	4.4	1.6	2.0
N	4	6	6	6
$\Delta^{\text{MAX}} [\text{°}]$	2.47	2.04	2.07	0.37
$\Delta^{\text{MEAN}} [\text{°}]$	1.38	1.00	0.94	0.22

v^P and v^S are the averaged P and S velocities, ρ is the density, A^P , A^{S1} and A^{S2} are the values of the P , $S1$ and $S2$ anisotropy strength, N is the number of real acoustic axes, and Δ^{MAX} and Δ^{MEAN} are the maximum and mean deviations between the approximate and exact directions of real acoustic axes. The anisotropy strength is defined as $a = 200(v^{\text{MAX}} - v^{\text{MIN}})/(v^{\text{MAX}} + v^{\text{MIN}})$, where v^{MAX} and v^{MIN} are the maximum and minimum phase velocities of the respective wave.

eral triclinic anisotropy. The strongest anisotropy is displayed by metapelite I with 6.8, 5.3 and 4.9 per cent for P , $S1$ and $S2$ waves, the weakest anisotropy is displayed by si-ga gneiss with values of 1.8, 3.4 and 2.0 per cent for P , $S1$ and $S2$ waves (see Table 2). These values indicate that the rocks under study display a rather weak anisotropy.

Figs 5 and 6 show the directional variation of the P -wave phase velocity and the variation of the difference between the $S1$ - and $S2$ -wave phase velocities for the rock samples under study. The figures also show directions of the real acoustic axes: metapelite I has four real acoustic axes, metapelite II, granulite and si-ga gneiss have equally six real acoustic axes. All the acoustic axes are conical. The acoustic axes were calculated using exact eqs (6a–c) and (7a–c) and also using approximate eqs (14a–c) in order to test the accuracy of the approximation. Table 2 summarizes the results of this test. The maximum difference between the exact and approximate directions of the acoustic axes is observed for metapelite I

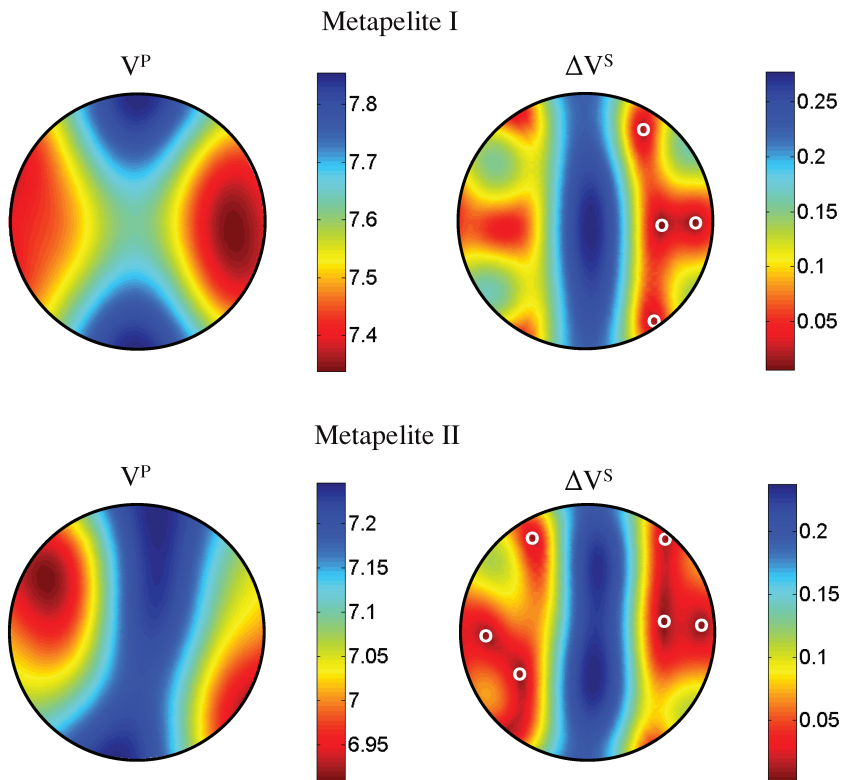


Figure 5. Directional variations of the P -wave phase velocity (left-hand plots) and of the difference between the $S1$ - and $S2$ -wave phase velocities (right-hand plots) for metapelite I and metapelite II. The velocities are in km s^{-1} . Equal area projection is used. The acoustic axes are marked by open white circles. For elastic parameters of the rock samples, see Table 1.

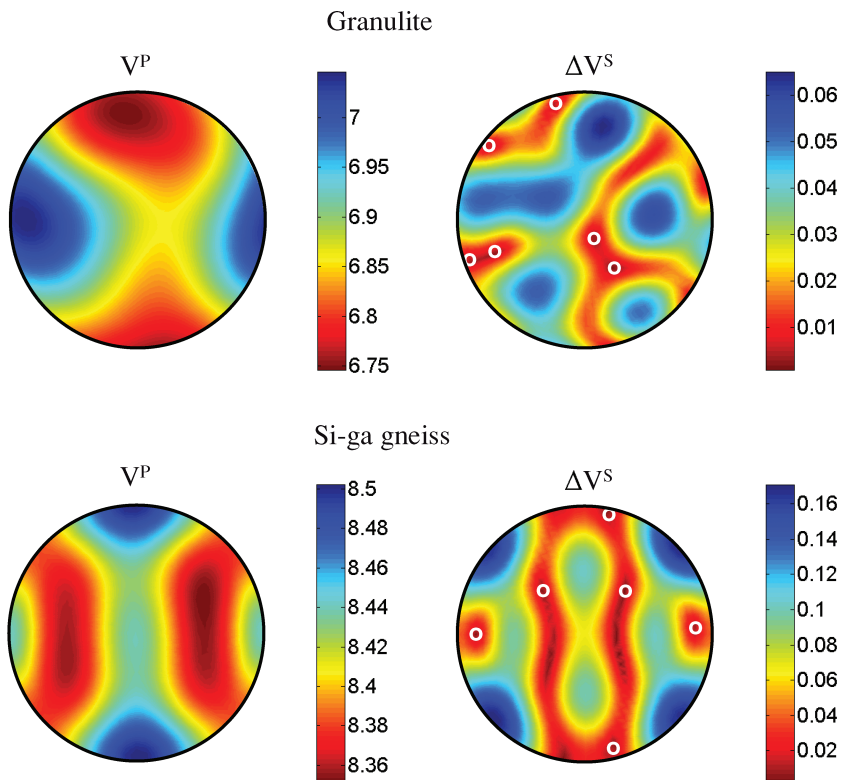


Figure 6. Directional variations of the P -wave phase velocity (left-hand plots) and of the difference between the $S1$ - and $S2$ -wave phase velocities (right-hand plots) for granulite and si-ga gneiss. The velocities are in km s^{-1} . Equal area projection is used. The acoustic axes are marked by open white circles. For elastic parameters of the rock samples, see Table 1.

and attains a value of about 2.5° . For other samples, the accuracy of approximate directions is higher. The best results are achieved for the si-ga gneiss, where the maximum deviation between the exact and accurate acoustic axes is only about 0.4° .

5 CONCLUSIONS

Acoustic axes can exist even under an infinitesimally weak anisotropy, and occur when slowness surfaces of the S1 and S2 waves touch or intersect. The maximum number of isolated acoustic axes in weak triclinic anisotropy is 16 as in strong triclinic anisotropy, hence a weak anisotropy condition does not reduce the maximum number of acoustic axes. However, media with 16 real-valued acoustic axes are very rare; the most frequent number of acoustic axes in weak triclinic anisotropy is much less, ranging between four and six (Vavryčuk 2005).

The directions of acoustic axes for strong triclinic anisotropy are calculated by solving two coupled polynomial equations of the sixth order in two variables. The system yields 36 real- or complex-valued solutions, from which 20 solutions are spurious and must be rejected. The real acoustic axes correspond to the degeneracy of homogeneous plane waves that propagate with a linear polarization. The complex acoustic axes correspond to the degeneracy of inhomogeneous plane waves that propagate with an elliptical polarization. The number and positions of real and complex acoustic axes depend on tensor b_{ijkl} , which defines anisotropy including its symmetry but they also depend on anisotropy strength controlled by parameter ε in (8).

Under the condition that strength of anisotropy is much less than the difference between the squares of the P and S velocities in the isotropic background, $\varepsilon/(\lambda + \mu) \rightarrow 0$, the order of the equations for acoustic axes is reduced from 6 to 5. This somewhat simplifies the problem and speeds up the calculation but not substantially. Due to the weak anisotropy condition, the acoustic axes are approximate and may deviate from the exact axes by several degrees for anisotropy strength about 5 per cent. The equations also yield some spurious solutions. These solutions are easily recognized because they are aligned in the coordinate planes. If also some true acoustic axes lie in the coordinate planes, then we obtain the total number of real and complex acoustic axes less than 16. In this case, the anisotropy must be rotated by an arbitrary angle and the procedure must be run again.

Although the weak anisotropy approximation does not simplify the problem of calculating the acoustic axes significantly, it can find some useful applications. The weak anisotropy approximation might be particularly advantageous when calculating acoustic axes under extremely weak anisotropy (anisotropy strength less than 0.1 per cent) because solving the exact equations may become numerically unstable or complicated to code. Also it can find applications in the inversion for anisotropy from the directions of acoustic axes.

ACKNOWLEDGMENTS

I thank Ivan Pšenčík for stimulating discussions on the subject, and Jules T. Browaeys and one anonymous reviewer for their comments. The work was supported by the Consortium Project SW3D ‘Seismic waves in complex 3-D structures’, and by the Grant Agency of the Academy of Sciences of the Czech Republic, Grant A3012309.

REFERENCES

- Alshits, V.I. & Lothe, J., 1979a. Elastic waves in triclinic crystals. I. General theory and the degeneracy problem, *Sov. Phys. Crystallogr.*, **24**, 387–392.
- Alshits, V.I. & Lothe, J., 1979b. Elastic waves in triclinic crystals. II. Topology of polarization fields and some general theorems, *Sov. Phys. Crystallogr.*, **24**, 393–398.
- Alshits, V.I. & Lothe, J., 2004. Some basic properties of bulk elastic waves in anisotropic media, *Wave Motion*, **40**, 297–313.
- Alshits, V.I., Sarychev, A.V. & Shuvalov, A.L., 1985. Classification of degeneracies and analysis of their stability in the theory of elastic waves in crystals, *J. Exper. Theor. Phys.*, **89**, 922–938 (in Russian).
- Babuška, V. & Cara, M., 1991. *Seismic Anisotropy in the Earth*, Kluwer Academic Publishers, London.
- Boulanger, Ph. & Hayes, M., 1998. Acoustic axes for elastic waves in crystals: theory and applications, *Proc. R. Soc. Lond. A* **454**, 2323–2346.
- Bulant, P. & Klimeš, L., 2004. Comparison of quasi-isotropic approximations of the coupling ray theory with the exact solution in the 1-D anisotropic ‘oblique twisted crystal’ model, *Stud. Geophys. Geod.*, **48**, 97–116.
- Červený, V., 2001. *Seismic Ray Theory*, Cambridge University Press, Cambridge.
- Chapman, C.H. & Shearer, P.M., 1989. Ray tracing in azimuthally anisotropic media—II. Quasi-shear wave coupling, *Geophys. J.*, **96**, 65–83.
- Coates, R.T. & Chapman, C.H., 1990. Quasi-shear wave coupling in weakly anisotropic 3-D media, *Geophys. J. Int.*, **103**, 301–320.
- Crampin, S. & Yedlin, M., 1981. Shear-wave singularities of wave propagation in anisotropic media, *J. Geophys.*, **49**, 43–46.
- Darinskii, B.M., 1994. Acoustic axes in crystals, *Crystallogr. Rep.*, **39**, 697–703.
- Every, A.G., 1986. Formation of phonon-focusing caustics in crystals, *Phys. Rev. B*, **34**, 2852–2862.
- Every, A.G., 1988. Classification of the phonon-focusing patterns of tetragonal crystals, *Phys. Rev. B*, **37**, 9964–9977.
- Farra, V., 2001. High-order perturbations of the phase velocity and polarization of qP and qS waves in anisotropic media, *Geophys. J. Int.*, **147**, 93–104.
- Farra, V., 2004. Improved first-order approximation of group velocities in weakly anisotropic media, *Stud. Geophys. Geod.*, **48**, 199–213.
- Farra, V., 2005. First-order ray tracing for qS waves in inhomogeneous weakly anisotropic media, *Geophys. J. Int.*, **161**, 309–324, doi:10.1111/j.1365-246X.2005.02570.x.
- Fedorov, F.I., 1968. *Theory of Elastic Waves in Crystals*, Plenum Press, New York.
- Fröberg, R., 1997. *An Introduction to Gröbner Bases*, John Wiley, New York.
- Grechka, V.Yu. & Obolentseva, I.R., 1993. Geometrical structure of shear wave surfaces near singularity directions in anisotropic media, *Geophys. J. Int.*, **115**, 609–616.
- Helbig, K., 1994. *Foundations of Anisotropy for Exploration Seismics*, Pergamon, New York.
- Holm, P., 1992. Generic elastic media, *Physica Scripta*, **T 44**, 122–127.
- Hurley, D.C. & Wolfe, J.P., 1985. Phonon focusing in cubic crystals, *Phys. Rev. B*, **32**, 2568–2587.
- Jech, J. & Pšenčík, I., 1989. First-order perturbation method for anisotropic media, *Geophys. J. Int.*, **99**, 369–376.
- Khatkevich, A.G., 1963. Acoustic axes in crystals, *Sov. Phys. Crystallogr.*, **7**, 601–604.
- Khatkevich, A.G., 1977. Classification of crystals by acoustic properties, *Sov. Phys. Crystallogr.*, **22**, 701–705.
- Klimeš, L. & Bulant, P., 2004. Errors due to the common ray approximations of the coupling ray theory, *Stud. Geophys. Geod.*, **48**, 117–142.
- Kravtsov, Yu.A. & Orlov, Yu.I., 1990. *Geometrical Optics of Inhomogeneous Media*, Springer-Verlag, New York.
- Mozhaev, V.G., Bosia, F. & Weihahn, M., 2001. Oblique acoustic axes in trigonal crystals, *J. Comput. Acoust.*, **9**, 1147–1161.

- Musgrave, M.J.P., 1970. *Crystal Acoustics*, Holden-Day, San Francisco.
- Musgrave, M.J.P., 1985. Acoustic axes in orthorhombic media, *Proc. R. Soc. Lond. A* **401**, 131–143.
- Pšenčík, I., 1998. Green's functions for inhomogeneous weakly anisotropic media, *Geophys. J. Int.* **135**, 279–288.
- Rümpker, G. & Thomson, C.J., 1994. Seismic-waveform effects of conical points in gradually varying anisotropic media, *Geophys. J. Int.* **118**, 759–780.
- Savage, M.K., 1999. Seismic anisotropy and mantle deformation: what have we learned from shear wave splitting?, *Rev. Geophysics*, **37**, 65–106.
- Shuvalov, A.L., 1998. Topological features of the polarization fields of plane acoustic waves in anisotropic media, *Proc. R. Soc. Lond. A* **454**, 2911–2947.
- Shuvalov, A.L., 2001. On the theory of plane inhomogeneous waves in anisotropic elastic media, *Wave Motion*, **34**, 401–429.
- Shuvalov, A.L. & Every, G., 1997. Shape of the acoustic slowness surface of anisotropic solids near points of conical degeneracy, *J. Acoust. Soc. Am.*, **101**, 2381–2383.
- Siegesmund, S., Kruhl, J.H. & Lüschen, E., 1996. Petrophysical and seismic features of the exposed lower continental crust in Calabria (Italy): field observations versus modelling, *Geotek. Forsch.*, **85**, 125–163.
- Thomsen, L., 1986. Weak elastic anisotropy, *Geophysics*, **51**, 1954–1966.
- Vavryčuk, V., 2001. Ray tracing in anisotropic media with singularities, *Geophys. J. Int.* **145**, 265–276.
- Vavryčuk, V., 2003a. Parabolic lines and caustics in homogeneous weakly anisotropic solids, *Geophys. J. Int.* **152**, 318–334.
- Vavryčuk, V., 2003b. Behavior of rays near singularities in anisotropic media, *Phys. Rev. B*, **67**, art. no. 54105.
- Vavryčuk, V., 2005. Acoustic axes in triclinic anisotropy, *J. Acoust. Soc. Am.*, **118**, 647–653.
- Weiss, T., Siegesmund, S., Rabbel, W., Bohlen, T. & Pohl, M., 1999. Seismic velocities and anisotropy of the lower continental crust: a review, *Pure Appl. Geophys.*, **156**, 97–122.
- Wolfe, J.P., 1998. *Imaging Phonons. Acoustic Wave Propagation in Solids*, Cambridge University Press, Cambridge.

APPENDIX A: THE CHRISTOFFEL TENSOR Γ FOR WEAK TRICLINIC ANISOTROPY

Inserting the weak anisotropy expansion, defined in eqs (8) and (9) into the definition of the Christoffel tensor (1), we obtain

$$\Gamma_{11} = (\lambda + 2\mu)n_1^2 + \mu(n_2^2 + n_3^2) + \varepsilon(b_{11}n_1^2 + b_{66}n_2^2 + b_{55}n_3^2 + 2b_{16}n_1n_2 + 2b_{15}n_1n_3 + 2b_{56}n_2n_3)$$

$$\Gamma_{22} = (\lambda + 2\mu)n_2^2 + \mu(n_1^2 + n_3^2) + \varepsilon(b_{66}n_1^2 + b_{22}n_2^2 + b_{44}n_3^2 + 2b_{26}n_1n_2 + 2b_{46}n_1n_3 + 2b_{24}n_2n_3)$$

$$\Gamma_{33} = (\lambda + 2\mu)n_3^2 + \mu(n_1^2 + n_2^2) + \varepsilon(b_{55}n_1^2 + b_{44}n_2^2 + b_{33}n_3^2 + 2b_{45}n_1n_2 + 2b_{35}n_1n_3 + 2b_{34}n_2n_3)$$

$$\Gamma_{12} = (\lambda + \mu)n_1n_2 + \varepsilon[b_{16}n_1^2 + b_{26}n_2^2 + b_{45}n_3^2 + (b_{12} + b_{66})n_1n_2 + (b_{14} + b_{56})n_1n_3 + (b_{25} + b_{46})n_2n_3]$$

$$\Gamma_{13} = (\lambda + \mu)n_1n_3 + \varepsilon[b_{15}n_1^2 + b_{46}n_2^2 + b_{35}n_3^2 + (b_{14} + b_{56})n_1n_2 + (b_{13} + b_{55})n_1n_3 + (b_{45} + b_{36})n_2n_3]$$

$$\Gamma_{23} = (\lambda + \mu)n_2n_3 + \varepsilon[b_{56}n_1^2 + b_{24}n_2^2 + b_{34}n_3^2 + (b_{25} + b_{46})n_1n_2 + (b_{36} + b_{45})n_1n_3 + (b_{23} + b_{44})n_2n_3]$$

APPENDIX B: POLYNOMIALS P_1 , Q_1 AND R_1

Polynomials P_1 , Q_1 and R_1 in (11a–c) are homogeneous polynomials of the sixth order in components of direction vector \mathbf{n} . They can be expressed as follows:

$$P_1 = n_3 p_{ij} n_1^i n_2^j n_3^{5-i-j}, \quad Q_1 = n_2 q_{ij} n_1^i n_2^j n_3^{5-i-j}, \quad R_1 = n_1 r_{ij} n_1^i n_2^j n_3^{5-i-j},$$

where summation over repeated indices is applied. Indices i and j run from 0 to 5 and their sum is less than or equal to 5. Coefficients p_{ij} read

$$\begin{aligned} p_{50} &= b_{56}, & p_{05} &= -b_{46}, \\ p_{20} &= -b_{45}, & p_{02} &= b_{45}, \\ p_{32} &= b_{24} - b_{14}, & p_{23} &= b_{25} - b_{15}, \\ p_{11} &= b_{55} - b_{44}, & p_{22} &= 3(-b_{26} + b_{16}), \\ p_{40} &= b_{45} + b_{36} - b_{16}, & p_{04} &= -b_{45} - b_{36} + b_{26}, \\ p_{41} &= b_{46} + b_{25} - b_{15}, & p_{14} &= -b_{56} + b_{24} - b_{14}, \\ p_{30} &= -b_{56} + b_{34} - b_{14}, & p_{03} &= b_{46} - b_{35} + b_{25}, \\ p_{21} &= -3b_{46} - b_{35} - b_{25} + 2b_{15}, & p_{12} &= 3b_{56} + b_{34} - 2b_{24} + b_{14}, \\ p_{31} &= -b_{55} + b_{44} + b_{23} - b_{13} - b_{12} + b_{11}, & p_{13} &= -b_{55} + b_{44} + b_{23} - b_{22} - b_{13} + b_{12} \end{aligned}$$

other coefficients being zero. Coefficients q_{ij} read

$$\begin{aligned}
 q_{50} &= b_{56} & q_{00} &= -b_{45} \\
 q_{03} &= b_{46} & q_{23} &= -b_{46} \\
 q_{13} &= -b_{44} & q_{21} &= 3(-b_{35} + b_{15}) \\
 q_{20} &= b_{36} - b_{16} & q_{30} &= b_{34} - b_{14} \\
 q_{01} &= -b_{46} + b_{35} - b_{25} & q_{10} &= -b_{56} + b_{34} - b_{14} \\
 q_{41} &= b_{46} + b_{25} - b_{15} & q_{40} &= b_{45} + b_{36} - b_{16} \\
 q_{02} &= b_{45} + b_{36} - b_{26} & q_{32} &= -b_{56} + b_{24} - b_{14} \\
 q_{22} &= -3b_{45} - b_{36} - b_{26} + 2b_{16} & q_{12} &= 3b_{56} - 2b_{34} + b_{24} + b_{14} \\
 q_{31} &= -2b_{55} + b_{44} + b_{23} - b_{13} - b_{12} + b_{11} & q_{11} &= 2b_{55} + b_{44} + b_{23} + b_{13} - b_{12}
 \end{aligned}$$

other coefficients being zero. Coefficients r_{ij} read

$$\begin{aligned}
 r_{00} &= -b_{45} & r_{05} &= b_{46} \\
 r_{30} &= b_{56} & r_{32} &= -b_{56} \\
 r_{31} &= -b_{55} & r_{12} &= 3(-b_{34} + b_{24}) \\
 r_{02} &= b_{36} - b_{26} & r_{03} &= b_{35} - b_{25} \\
 r_{01} &= -b_{46} + b_{35} - b_{25} & r_{10} &= -b_{56} + b_{34} - b_{14} \\
 r_{04} &= b_{45} + b_{36} - b_{26} & r_{14} &= b_{56} - b_{24} + b_{14} \\
 r_{20} &= b_{45} + b_{36} - b_{16} & r_{23} &= -b_{46} - b_{25} + b_{15} \\
 r_{21} &= 3b_{46} - 2b_{35} + b_{25} + b_{15} & r_{22} &= -3b_{45} - b_{36} + 2b_{26} - b_{16} \\
 r_{11} &= b_{55} + 2b_{44} + b_{23} + b_{13} - b_{12} & r_{13} &= b_{55} - 2b_{44} - b_{23} + b_{22} + b_{13} - b_{12}
 \end{aligned}$$

other coefficients being zero. Matrix b_{IJ} , $I, J = 1, \dots, 6$ is the two-index notation of tensor b_{ijkl} (see Musgrave 1970, eq. 3.13.4).